Atmos. Chem. Phys., 17, 9645–9663, 2017
https://doi.org/10.5194/acp-17-9645-2017

Atmospheric Chemistry and Physics
Open Access
EGU

Importance of the Saharan heat low in controlling the North Atlantic free tropospheric humidity budget deduced from IASI δD observations

Jean-Lionel Lacour[1,4], Cyrille Flamant[1], Camille Risi[2], Cathy Clerbaux[1,3], and Pierre-François Coheur[3]

[1]UPMC Univ. Paris 06; Université Versailles St-Quentin, LATMOS-IPSL, Paris, France
[2]UPMC Univ. Paris 06; UMR8539, CNRS/INSU, LMD-IPSL, Paris, France
[3]Spectroscopie de l'Atmosphère, Service de Chimie Quantique et Photophysique, Université Libre de Bruxelles (ULB), Brussels, Belgium
[4]Institute of Earth Sciences, University of Iceland, Reykjavik, Iceland

Correspondence to: Jean-Lionel Lacour (jean-lionel.lacour@latmos.ipsl.fr)

Received: 16 February 2017 – Discussion started: 21 March 2017
Revised: 9 July 2017 – Accepted: 10 July 2017 – Published: 10 August 2017

Abstract. The isotopic composition of water vapour in the North Atlantic free troposphere is investigated with Infrared Atmospheric Sounding Interferometer (IASI) measurements of the D / H ratio (δD) above the ocean. We show that in the vicinity of West Africa, the seasonality of δD is particularly strong (130 ‰), which is related with the influence of the Saharan heat low (SHL) during summertime. The SHL indeed largely influences the dynamic in that region by producing deep turbulent mixing layers, yielding a specific water vapour isotopic footprint. The influence of the SHL on the isotopic budget is analysed on various time and space scales and is shown to be large, highlighting the importance of the SHL dynamics on the moistening and the HDO enrichment of the free troposphere over the North Atlantic. The potential influence of the SHL is also investigated on the inter-annual scale as we also report important variations in δD above the Canary archipelago region. We interpret the variability in the enrichment, using backward trajectory analyses, in terms of the ratio of air masses coming from the North Atlantic and air masses coming from the African continent. Finally, the interest of IASI high sampling capabilities is further illustrated by presenting spatial distributions of δD and humidity above the North Atlantic from which we show that the different sources and dehydration pathways controlling the humidity can be disentangled thanks to the added value of δD observations. More generally, our results demonstrate the utility of δD observations obtained from the IASI sounder to gain insight into the hydrological cycle processes in the West African region.

1 Introduction

In the North Atlantic, the free tropospheric humidity is the result of a complex interplay between moistening and dehydrating processes of air parcels originating from different sources. While the large-scale subsidence largely controls the dryness of the subtropics, numerous other processes have been shown to moisten the subsiding air, such as large-scale transport from the tropics (Sherwood, 1996) or vertical mixing associated with convection, or evaporation of condensate in the convective towers (Sun and Lindzen, 1993). Due to the difficulty of disentangling the relative contributions of these processes and of the different sources, controls on tropospheric humidity remain imprecise. Additionally, these different sources and processes may be affected by the modulation of regional environmental influences such as the migration of the Intertropical Convergence Zone (ITCZ) (Wilcox et al., 2010), the activity of the Saharan heat low (SHL) (Lavaysse et al., 2010) or the West African Monsoon and associated mesoscale convective systems. Furthermore, the subtropical North Atlantic is a particularly climate-sensitive

area (Spencer and Braswell, 1997) as the radiative forcing associated with changes in water vapour is the strongest in the free troposphere (Held and Soden, 2000). Efforts in understanding the controls on the North Atlantic humidity are thus crucial.

The measurement of water vapour isotopologues has proved to be a helpful observational diagnostic to study the atmospheric moistening–dehydrating processes in a novel way (e.g. Worden et al., 2007; Frankenberg et al., 2009; Risi et al., 2012; Yoshimura et al., 2014; Tuinenburg et al., 2015; Galewsky et al., 2016). This is because the water isotopologues (HDO, $H_2{}^{16}O$, $H_2{}^{18}O$) preferentially condense–evaporate during the phase changes of water, and therefore their isotopic ratio is sensitive to key processes of the hydrological cycle such as air mass mixing (Galewsky et al., 2007), convection (Risi et al., 2008), and transport (Galewsky and Samuels-Crow, 2015). The observation of water isotopologues in the vapour thereby provide useful information on the processes that affected the air masses downwind. While the number of δD ($\delta D = 1000 \times [(HDO/H_2O)/Rsmow - 1]$, Rsmow being the $HDO\,/\,H_2O$ ratio in the standard mean ocean waters) measurements has increased this last decade (e.g. Lacour et al., 2012; Worden et al., 2012; Schneider et al., 2016), it is necessary to understand the factors controlling their variations in order to apprehend their utility for studying hydrological processes. With its demonstrated capabilities to provide δD measurements in the free troposphere (Schneider and Hase, 2011; Lacour et al., 2012, 2015), the Infrared Atmospheric Sounding Interferometer (IASI) flying onboard MetOp has played a key role in supplying δD observations for a decade. IASI has the advantage of making about 1.3 million measurements a day, which almost ensures one measurement everywhere on the globe twice a day. Up to now, IASI δD retrievals have been sparsely used for geophysical analyses (Bonne et al., 2015; Tuinenburg et al., 2015).

In this study, we use δD and humidity profiles retrieved from IASI at ULB/LATMOS (Lacour et al., 2012, 2015) to explore the isotopic signal on various time and space scales above the North Atlantic near the West African coast and we interpret their seasonal to inter-annual variability as well as their spatial variations. This enables us to investigate the potential of such observations to improve our understanding of the moistening processes in this region. Because the retrieval of δD above deserts is difficult due to uncertainties in the surface emissivity and the presence of dust, we have chosen to not analyse the measurements above the Sahara. Nevertheless, because of the integrated nature of δD, we show that some information can be derived from the δD signature of air parcels coming from the desert. Former studies have already been dedicated to the interpretation of isotopic variations observed in precipitation and in water vapour in West Africa (Frankenberg et al., 2009; Risi et al., 2010; Okazaki et al., 2015) by combining models with observations, but solely focusing on the role of convection. From in situ measurements at Izana, González et al. (2016) have shown that different air mass pathways could be detected in H_2O–δD pair distribution. The sensitivity of δD observations to different moisture pathways has also been reported from ground-based Fourier transform infrared (FTIR) and IASI measurements (Schneider et al., 2015) within the MUSICA project (Schneider et al., 2016). Here, from IASI H_2O and δD ULB/LATMOS retrieval products, we use this property of isotope to first show that the SHL – which is a key component of the West African Monsoon system – has a large influence on the budget of water isotopologues above the North Atlantic in summertime, when the SHL is most active, leading to a strong seasonality of δD. Then, we present inter-annual variability in the isotopic composition above the Canary archipelago region (CAR) and analyse the causes of the variability. Finally, we detail the spatial variations in water vapour and its isotopic composition above the North Atlantic for July 2012 and discuss the different sources and dehydration pathways controlling the free tropospheric humidity.

In Sect. 2 we present the IASI datasets and the different numerical weather prediction model reanalyses that we have used and we provide some guidance on the interpretation of δD–humidity variations. We analyse the seasonal and inter-annual δD variations observed above the CAR in Sects. 3 and 4, respectively. Then in Sect. 5, we describe the spatial distribution of δD observed in July 2012. Finally, the results are discussed in the conclusion section.

2 Data and methods

2.1 IASI δD retrievals

This study is mainly based on H_2O and δD profiles derived from IASI radiance measurements (Lacour et al., 2012, 2015) from the retrieval processor developed at ULB/LATMOS. IASI is a Fourier transform spectrometer onboard the MetOp platform measuring the thermal infrared emission of the Earth and the atmosphere (Clerbaux et al., 2009). The high-quality spectra (good spectral resolution $-0.5\,cm^{-1}$ – and low radiometric noise) allow the retrieval of information on H_2O and δD in the troposphere after an inversion procedure following the optimal estimation method (Rodgers, 2000) adapted for the requirements of δD retrieval (Worden et al., 2006; Schneider et al., 2006). With respect to supplying δD observations in the free troposphere, IASI is the unique successor of the Tropospheric Emission Spectrometer (TES) instrument, which has been used in many isotopic application studies (i.e. Worden et al., 2007; Risi et al., 2010, 2013). IASI with its high spatio-temporal sampling (a measurement almost everywhere on the globe, twice a day) is of great interest for studies on short-term variations in δD (Bonne et al., 2015; Tuinenburg et al., 2015) and for an optimal sampling of δD natural variability (Lacour et al., 2015).

The δD profiles retrieved from IASI have limited information on the vertical, with degrees of freedom vary-

ing between 1 and 2 depending on the local conditions (thermal contrast, temperature, and humidity profiles; e.g. Pommier et al., 2014). In general, the maximum of sensitivity of the retrieval lies in the free troposphere between 3 and 6 km. For our analysis we use only the retrieved δD profiles that have more than 1.5 degrees of freedom and that yield a maximum of sensitivity between 4 and 6 km. It is also important to mention that the retrieved profiles of δD and humidity are not exactly representative of the same atmosphere, the humidity profile having more vertical information than δD. It is thus important to keep in mind that when δD–q pairs are considered, the δD estimate is representative of a thicker layer than the q estimate. On an individual basis, the observational error on δD between 4 and 6 km has been estimated and cross-validated to 38 ‰ (Lacour et al., 2015). When several retrieved values are averaged (from N measurements), this error is reduced by a factor $\sqrt{N}$. Because of the large number of IASI measurements, there is presently no near-real-time processing of IASI radiances for δD. The availability of this quantity is thus limited. In this study we use three different datasets to investigate the isotopic characteristics of water vapour in the North Atlantic:

- a 5-year (2009–2013) dataset above the CAR (26–30° N, 18–14° W) with an average of 65 measurements available per day;
- a 1-year dataset (2011) along a latitudinal band of narrow longitudinal extent (0–60° N, 30–25° W), which is used in Sect. 3.4 to evaluate the variations in δD seasonality along the West African coast;
- a 1-month dataset (July 2012) above the North Atlantic (0–40° N, 40–5° W), which is also used to illustrate the spatial extent of the influence of the SHL (Sect. 3.4) and to analyse the different sources and processes controlling the humidity above the North Atlantic in Sect. 5.

These data are used on different timescales from the individual observation to monthly averages. Daily means are obtained by averaging individual observations and monthly averages are obtained from the daily averages.

There exists another δD retrieval processor from IASI spectra (Schneider and Hase, 2011) developed within the MUSICA project (Schneider et al., 2016), which we do not use in this study; a brief summary of the differences of the processors is given in the Appendix of Schneider et al. (2016). The MUSICA MetOp IASI data have already been used previously for documenting the different moisture pathways in the subtropical North Atlantic region (Schneider et al., 2015).

2.2 TES δD retrieval

In order to derive a climatology of δD seasonality on a global scale, we also used δD profiles retrieved from the Tropospheric Emission Spectrometer (TES) measurements (Worden et al., 2012). The TES instrument is, like IASI, a thermal infrared sounder but with a better spectral resolution, which makes it more sensitive to the lower troposphere. The observational error on δD retrieved values from TES has been evaluated to ± 30 ‰ (Worden et al., 2012; Herman et al., 2014). The spatio-temporal sampling is however lower than IASI. Nevertheless, δD retrievals from TES have been available since September 2009 and allow for global analysis of δD.

2.3 Backward trajectory analyses and reanalysis data

To help in the interpretation of δD data, we use backward trajectory calculations from the Hybrid Single-Particle Lagrangian Integrated Trajectory (HYSPLIT) model (Stein et al., 2015) in which NCEP GDAS (Global Data Assimilation System) reanalyses (Kleist et al., 2009) have been used as the meteorological fields. Backward trajectories have been mainly used in the analysis of the dataset above the CAR. Three trajectories arriving at 26, 28, and 30° N at the longitudinal centre of the box are computed for each day of IASI observation. In our analysis the trajectories we used are initialized from midday at an altitude of 5.5 km. As the retrieved values of IASI are sensitive over a large layer of the true δD variations, we checked that the air trajectories arriving at 4.5 and 3.5 km were similar. This is shown in the Appendix for the year 2011. It is also shown that we do not expect temporal mismatch to significantly affect the air parcel history. We also used ECMWF (Dee et al., 2011) and MERRA (Rienecker et al., 2011) reanalysis data to characterize atmospheric dynamics.

2.4 Background on δD analysis

Variations in δD are to a first order tied to those in absolute humidity (here we use water vapour mixing ratio, noted as q). For this reason the interpretation of the information contained in δD is generally done in the δD–q space, which allows for a joint analysis of their variations. While the interpretation of δD–q pairs can be complicated as numerous processes can produce the same δD–q combination, simple models are helpful to understand their position in the δD–q space (Noone, 2012). The isotopic depletion of water vapour that undergoes condensation at equilibrium can be described by a Rayleigh distillation model as

$$\delta\mathrm{D} = (\alpha - 1)\ln\frac{q}{q_0} + \delta\mathrm{D}_0, \quad (1)$$

in which q_0 and $\delta\mathrm{D}_0$ are the specific humidity and the isotopic composition of the water vapour source, and α is the coefficient of fractionation. This model is shown in Fig. 1 for two different sources of water vapour (purple lines). A Rayleigh model with a tropical water vapour source can generally be used to describe the lower limit of the domain of existence of δD–q pairs. The superior limit of this domain

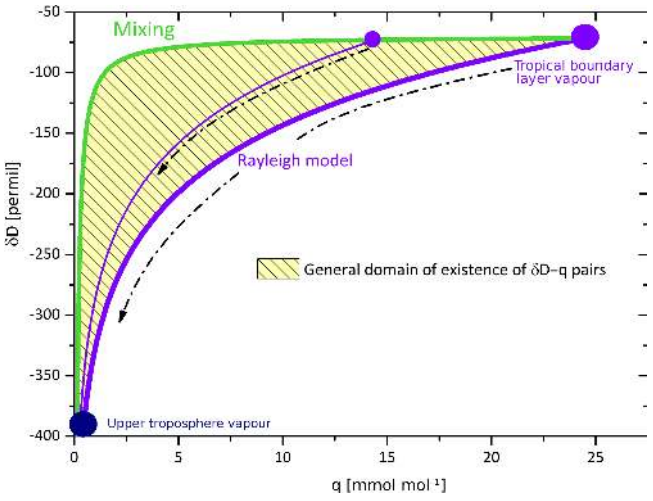

Figure 1. Simple models describing the domain of existence of δD–q pairs. The two purple curves describe the progressive depletion of a tropical boundary layer source and a drier one according to a Rayleigh distillation. The green curve describes the mixing between humidity from the tropical boundary layer source with humidity of the upper troposphere.

can be described by a mixing model between depleted and dry air from the upper troposphere that mixes with enriched and humid air from the tropical boundary layer (green line in Fig. 1). The mixing between sources A and B produces a resulting air parcel of mixing ratio q, which is the weighted average of the mixing ratio of the two air parcels:

$$q = f[H_2O]_A + (1 - f)[H_2O]_B, \quad (2)$$

with f, the mixing fraction. The resulting ratio of isotopologues is given as (Galewsky and Hurley, 2010)

$$R_{mix} = \frac{f[HDO]_A + (1 - f)[HDO]_B}{f[H_2O]_A + (1 - f)[H_2O]_B}. \quad (3)$$

The mixing model is shown in green in Fig. 1. Mixing and distillation of water vapour from different sources can occur over a wide range of combinations and produce δD–q pairs in between these two boundary models. Note that intense convective activity over depletes water vapour through raindrop re-evaporation and δD–q pairs can be found below the Rayleigh distillation model (Worden et al., 2007).

3 Seasonal variations: influence of the SHL on δD in the subtropical North Atlantic

3.1 Seasonal cycle of water vapour and its isotopic composition over the CAR

Figure 2a shows the composite (2009–2013) seasonal cycles of specific humidity and its isotopic composition at 5.5 km above the CAR. The troposphere is moistened from April to August as the large-scale subsidence weakens due to the northward migration of the ITCZ. Then, it progressively dries as the ITCZ retreats south. Interestingly, the δD composition of water vapour does not follow the exact same cycle as humidity: the air masses are indeed progressively enriched (5 ‰ per month) from January to June before exhibiting an abrupt enrichment from June to July (110 ‰ in 1 month). The enrichment persists throughout August with values nearly as high as in July. Afterwards, the HDO content rapidly decreases by $\sim$ 130 ‰ from August to November, while humidity stays high until October. This strong seasonality in δD values is particularly striking and exceeds the seasonality generally found elsewhere (see Sect. 3.4). The period of enrichment in HDO over the CAR appears to coincide with the period when the SHL is present over the western Sahara as the climatological onset of the SHL occurs at the end of June and the SHL retreats toward the south at the end of September (Lavaysse et al., 2009). In the following, we conduct our analyses with the aim of understanding the factors controlling this strong seasonality and its link with the SHL. Figure 2 (panel b) also shows important inter-annual variability observed in the δD signal not correlated to the humidity variability. We focus on the inter-annual variations in Sect. 4.

3.2 The Saharan heat low and the associated atmospheric dynamics

In summer, strong heating of the Saharan surface creates a low pressure system (SHL), which enhances convergence in the low levels (see panel a of Fig. 3 illustrating the low-level circulation for July 2012). In the lower troposphere, the cyclonic circulation around the SHL simultaneously strengthens the south-westerly monsoon flow east of its centre and the north-easterly Harmattan flow to the west. The near-surface convergence generates enhanced rising motion in an environment prone to dry convection, leading to the formation of deep well-mixed boundary layers, whose tops often reach 600 hPa or higher. The divergent circulation at the top of the SHL generates an anticyclonic circulation in the middle troposphere, which contributes to the intensification of the African easterly jet (AEJ) further south (Thorncroft and Blackburn, 1999) and which is responsible for the horizontal transport of continental air masses above the Atlantic. The middle tropospheric circulation for July 2012 represented in Fig. 3 shows how the anticyclonic circulation contributes to strengthening the AEJ and to bringing mid-level air masses from north-western Africa over the north-eastern Atlantic.

The development of a heat low due to the surface heating has several consequences on the atmospheric dynamics. In the summer, once the SHL settles in, the top of the Saharan air boundary layer (SABL) can reach an altitude of 6 to 7 km ($\sim$ 550 hPa) due to the enhanced near-surface convergence in the SHL region. The SABL is fully developed in the late afternoon (Chaboureau et al., 2016). Dur-

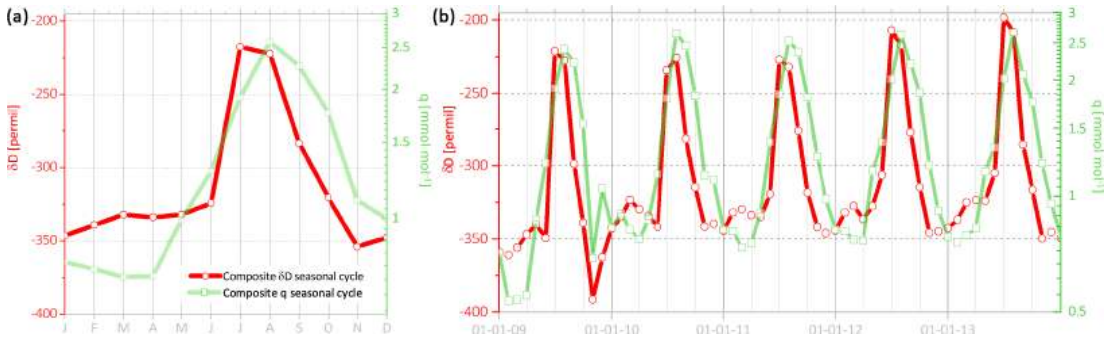

Figure 2. **(a)** Composite seasonal cycles of δD (red) and specific humidity (green) above the CAR for the 2009–2013 time period. **(b)** Monthly variations in δD (red) and specific humidity (green) above the CAR for the 2009–2013 time period.

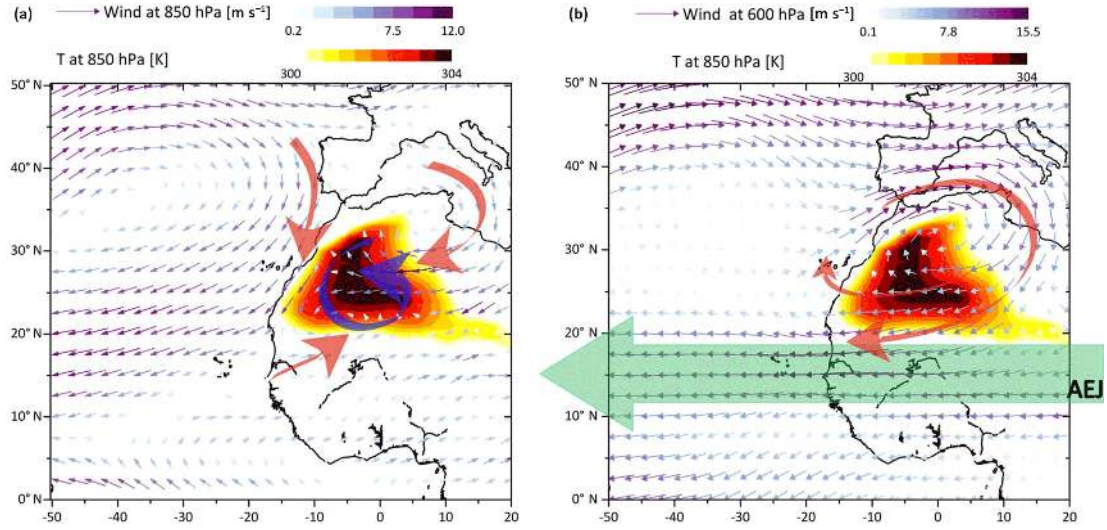

Figure 3. Low-level **(a)** and mid-level **(b)** circulation associated with the SHL. The location of the SHL is indicated by the temperature field at 850 hPa above 300 K in both panels. The arrows represent wind fields at 850 hPa **(a)** and 600 hPa **(b)**. In panel **(a)**, the red arrows indicate the different sources converging in the depression and the blue arrow represents the anticyclonic circulation associated with the SHL. In panel **(b)**, the red arrows shows how the anticyclonic circulation is divided into a part strengthening the AEJ.

ing most of the day, while the mixed layer is developing, the characteristics of air masses in the upper part of the SABL (the residual layer) are controlled by advection from the east (Flamant et al., 2007, 2009; Chaboureau et al., 2016). As the warm and dry air moves off the African coast, the SABL rises and becomes the Saharan Air Layer (SAL) undercut by the cool and moist marine boundary layer. The SAL contributes to important dust transport over the Atlantic (e.g. Prospero and Carlson, 1972) and has been widely studied by the aerosol community (e.g. Ben-Ami et al., 2009; Rodríguez et al., 2011).

The intensity of the SHL also has an influence on deep convection over the Sahel (Lavaysse et al., 2010) and hence on the precipitation over the area. Lavaysse et al. (2010) have indeed shown that during anomalously warm SHL phases (SHL more intense than on average) the south-westerly monsoon flow is reinforced over the central and eastern Sahel, leading to enhanced deep convection. At the same time, deep convection is reduced over the western Sahel. Evan et al. (2015) and Lavaysse et al. (2016) have further shown that the SHL intensity has increased (due to the warming of the Sahara) in the 2000s compared to the 1980s, explaining the increase in precipitation observed in the central and western Sahara in the recent years (Panthou et al., 2014). On inter-annual scales, the intensity of the SHL can significantly modulate deep convection over the Sahel. Furthermore, the diverging anticyclonic circulation at the top of the SHL influences the intensity of the AEJ and the westward transport of moisture.

3.3 Relationship between the SHL and the summer enrichment over the Atlantic

To gain insights into the processes leading to the seasonal evolution of the isotopic composition of water vapour shown

in Fig. 2, we analyse the monthly δD–q diagrams from March to October 2012 in Fig. 4a using Rayleigh and mixing models (the same models as in Fig. 1 are shown for simplicity) and using all the IASI observations. The colour indicates the gradient of temperature computed between 5.5 and 1.5 km. In parallel, we provide monthly analyses of air mass trajectories reaching the CAR from HYSPLIT backward trajectory analyses (Fig. 4b). Air masses arriving at the CAR from lower altitudes are identified by dark to light orange lines while air masses coming from higher altitudes are identified by dark to light purple lines. The bottom panels of Fig. 4 (Fig. 4c) show the monthly temperature at 850 hPa over the domain, this variable being a proxy of the SHL location over the Sahara.

The δD–q diagrams in the top panel of Fig. 4 show a clear change in the repartition of the δD–q pairs from May to June. In May, air masses are characterized by low δD values and a wide range of specific humidity. These observations are localized close to or below the Rayleigh model or close to the dry end of the mixing model. The measurements below the Rayleigh model are associated with air masses coming from the tropics and from lower altitudes and can thus be explained by convective processes (e.g. Worden et al., 2007). In June there is a clear separation of the measurements in two clusters, with the cluster of enriched air masses close to the mixing model and the cluster of depleted air masses located between the Rayleigh model and the mixing model. The two clusters also indicate a clear change in the temperature gradients, highlighting two different atmospheres. In July, only the enriched cluster is seen with high temperature gradients; it is associated with larger specific humidity values. The same applies in August with slightly more depleted values. In September and October, the observations are located in the left corner of the diagram (more depleted and less humid). The distribution of the δD–q observations in October 2012 is similar to that of May 2012. This situation then persists until the end of the year (not shown here). In summer, the position of the δD–q pairs along the mixing model suggests important mixing between dry, depleted air parcels and moist, enriched ones. Additionally, the fact that they are localized on the moist branch of the mixing model indicates a mixing for which the proportion of the moist term is quite important; this is surprising at an altitude of 5.5 km.

The backward trajectories shown in the middle panel of Figure 4 highlight that the shift in the cluster of δD–q pairs towards higher δD values (from -300 to -100 ‰) corresponds to a change in the origin of the air mass. During most of the year, the main origin of the air masses arriving in the CAR is the upper troposphere above the Atlantic Ocean. Conversely, from June to August, the air masses come from lower altitudes and from a more localized area in the western Sahara. The situation in June, which is characterized by a HDO-enriched δD–q cluster and an HDO-depleted one, is particularly noteworthy and can be explained with the trajectory analysis: the depleted cluster would be associated with air masses coming from the Atlantic and from higher altitudes, while the enriched cluster would correspond to the air masses coming from the African continent and from lower altitudes. Such differences in the δD–q distributions due to different origins of air masses have already been reported from in situ measurements in González et al. (2016).

The bottom panels in Fig. 4 indicate that the change in air mass trajectories is concomitant with the onset of the SHL, i.e. the installation of the SHL over the western and central Sahara (Lavaysse et al., 2009). The concomitant shift of δD–q pair clusters from a δD value of ~ -300 ‰ to a value of ~ -100 ‰, with the change in air mass trajectories and the installation of the SHL above West Africa shown here for the year 2012, is observed for the entire 2009–2013 period, with some differences that are discussed in Sect. 4. Therefore, it appears that the isotopic signal in the water vapour above the Atlantic is strongly influenced by the development of the SHL.

Figure 5 shows different diagnostics of the state of the atmosphere associated with different combinations of isotopic composition and water vapour content. We plot in Fig. 5a the daily average (not the individual observations as in Fig. 4) δD–q variations for the period 2009–2013 and select four boxes defining contrasting conditions: dry and depleted (orange box), dry and enriched (cyan box), humid and depleted (purple box), and humid and enriched (green box). The green box corresponds to the situation found in July–August with air masses coming from the Sahara, the purple box corresponds to depleted values associated with air masses coming from the tropical Atlantic at the end of the summer, and the cyan and orange boxes correspond to most of the daily values found during most of the year and are generally associated with air parcels coming from the North Atlantic. The number of days per month corresponding to each box is plotted in Fig. 5b. The average precipitation amount (computed from the reanalysis at a time step of 3 h) along the backward trajectories is also shown in Fig. 5c. For each box we plot the composite profiles of the temperature (Fig. 5d), specific humidity (Fig. 5e), relative humidity (Fig. 5f), and Richardson number (Fig. 5g).

For all variables, the ones corresponding to the green and purple boxes strongly deviate from the majority of the observations (characterized by the blue and orange boxes in which most of the δD–q pairs lie). The humidity profiles corresponding to the purple box show high humidity (relative and specific) values, which strongly suggest convective processes at play, furthermore confirmed by the precipitations found along the backward trajectory (Fig. 5c). In the case of the enriched and humid values, corresponding to the summer enrichment (green box), the different profiles characterize a very particular atmosphere. The specific humidity profile has very high values close to the surface, which rapidly decrease with altitude. The relative humidity profile also shows very high values in the first layer of the atmosphere compared to very dry values up to around 550 hPa. The temperature pro-

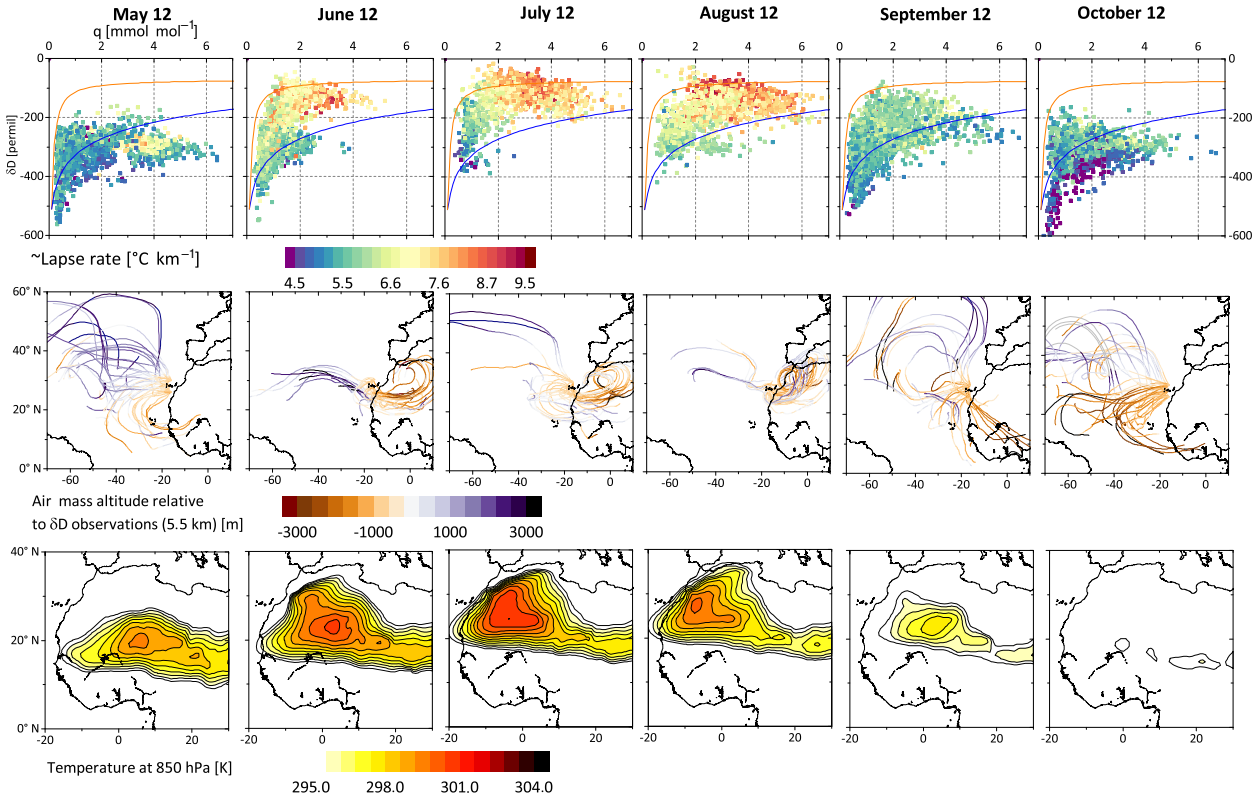

Figure 4. Top panels: δD and q variations from May to October 2012. All IASI individual observations within the box are shown. The mixing (orange line) and Rayleigh models (blue) are also shown. The temperature lapse rate is given by the colour scale. Middle panels: backward trajectory analyses of the air parcels arriving at the CAR from May to October 2012. The altitude of the air parcels is indicated relative to the observation altitude (5.5 km). Bottom panels: monthly temperatures at 850 hPa from May to October 2012.

file presents an inversion layer followed by a warm layer. The Richardson number profile indicates very stable values within a thick layer between 900 and 550 hPa. All these features are in fact characteristic of the thermodynamical structure of a deep SAL moving above a thin marine boundary layer. In Fig. 6 we show the development of the deep SABL during the year. One can see that the height of the boundary layer reaches the altitude of IASI sensitivity from June to the end of August. It is however only by the end of June when the air masses originating from the upper part of the atmospheric boundary layer (ABL) above the Sahara are transported above the Atlantic that the δD signal above the CAR rapidly increases. The seasonality of δD observed in the free troposphere above the CAR can thus be explained by the development of deep ABL associated with the settling of the SHL over the western Sahara. The latter acts to efficiently mix dry upper tropospheric air with air from the boundary layer.

Please note that the four boxes delimiting the different δD–q signatures (here defined arbitrarily) are very similar to the dissociation of in situ δD–q measurements by González et al. (2016) based on the temperature of the last condensation of air parcels.

3.4 Spatial extent of the SHL influence

As the high seasonality in the water isotopic composition observed at the CAR is closely associated with the activity of the SHL, it can serve as a diagnostic to evaluate the spatial influence of the SHL. In Fig. 7a we first present the seasonality in the δD signal (defined as $\bar{\delta}\mathrm{D}_{\mathrm{July–August}} - \bar{\delta}\mathrm{D}_{\mathrm{January–February}}$) observed from the TES instrument. We use the TES δD data here as they are available over a longer time period than the IASI dataset considered here and on a global scale. We plot the seasonality of δD as a zonal mean with its associated standard deviation, calculated for the 2005–2010 period. The seasonality observed off the West African coast, on an entire latitudinal band of narrow longitudinal extent (30–25° W), is also drawn in orange. The latter exhibits a sharp maximum around 22° N, which exceeds values found globally. We attribute this high seasonality as the result of the SHL activity and therefore suggest that its influence on the isotopic budget of water vapour extends over a large part of the North Atlantic. Figure 7b shows the same as Fig. 7a but for IASI data in 2010. These also show the enrichment in July–August from 15 to 30°. The bottom panel of Fig. 7, which shows the seasonality for the specific humidity (in percent), reveals a

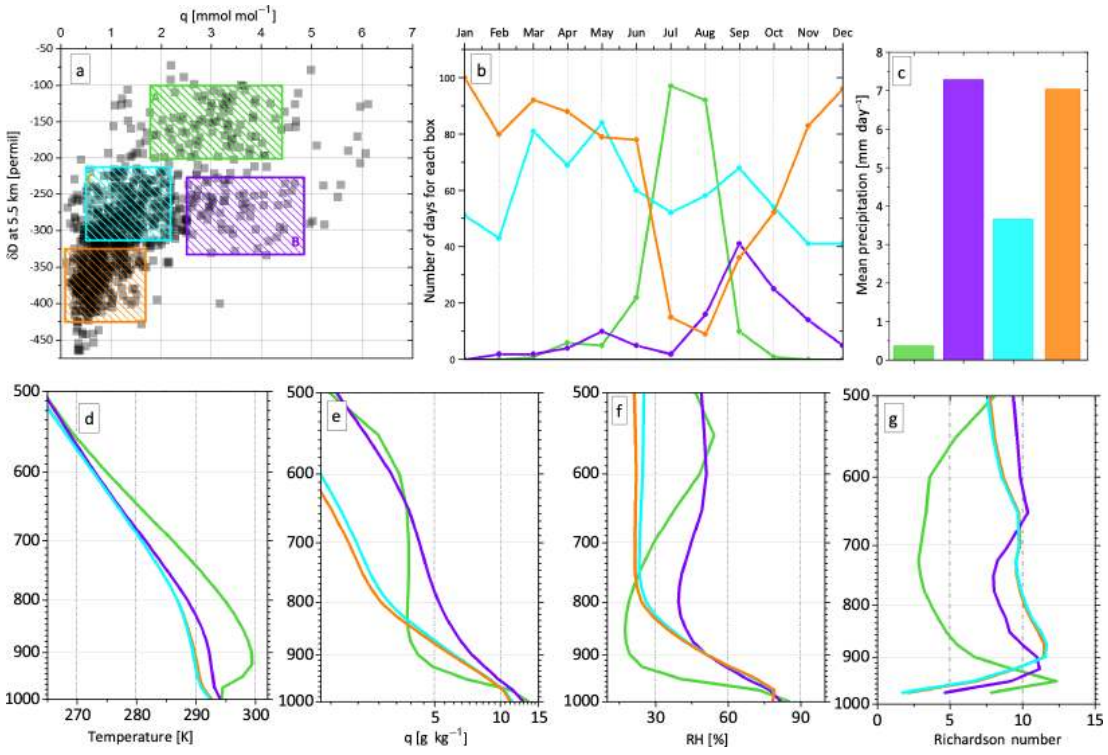

Figure 5. Dynamical characterization of the δD–q space. **(a)** Daily variations in δD and q for the entire 2009–2013 period with different boxes in which composite profiles have been derived from different geophysical parameters (see text for details). **(b)** Number of days per month found within each box. **(c)** Mean precipitation along the backward trajectories. Panels **(d)** to **(h)** show composite profiles of temperature (K), specific humidity (g kg^{-1}), relative humidity, and Richardson number (from MERRA reanalysis).

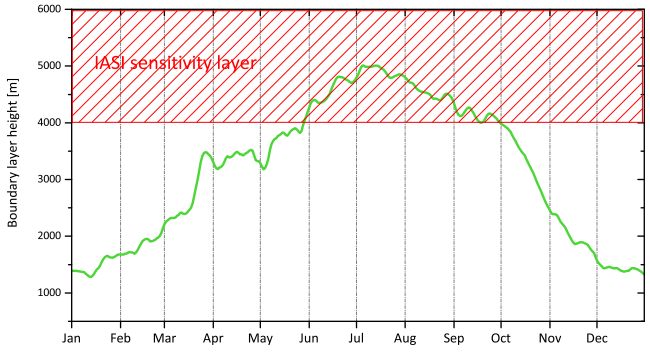

Figure 6. Development of deep boundary layers during summer above the Sahara (7° W–5° E, 20–30° N). Boundary layer heights are extracted from ECMWF ERA-Interim reanalysis and are averaged from 2009 to 2013.

different behaviour. The observed maximum in δD, which does not correspond to the maximum in humidity, can also be interpreted as the signature of the SHL, as mixing processes produce a stronger isotopic signal for a given specific humidity than any other hydrological processes (Galewsky and Hurley, 2010; Noone, 2012).

The differences between humidity and δD are also clearly visible in the spatial distributions of δD and q for July 2012 shown in Fig. 8. The water vapour distribution strongly differs from its isotopic composition as the maximum in Deuterium enrichment does not appear along the ITCZ, where high δD values are generally associated with high humidity in convective areas (Risi et al., 2012), where convection acts to bring enriched air masses to higher altitudes. Instead, we find the maximum of enrichment further north, around 20° N at the northern edge of the AEJ, for a wide range of specific humidity values.

The spatial pattern drawn by the high seasonality of δD can be linked to the dynamics of the SAL. Tsamalis et al. (2013) have shown that the SAL displays a clear seasonal cycle (both in latitudinal extent and in vertical structure), using 5 years of data from the space-borne Cloud-Aerosol Lidar with Orthogonal Polarization (CALIOP) (Winker et al., 2010). The SAL occurs at higher altitudes and farther north during the summer than during winter. Near the African coastline, the SAL is found between 5 and 30° N in summer, its northern edge being observed just north of the Canary Islands. The northern edge of the SAL migrates to 15° N during the winter and is generally observed to be south of the Canary Islands from September to May (see Fig. 2 of Tsamalis et al., 2013). During the summer, the SAL is found

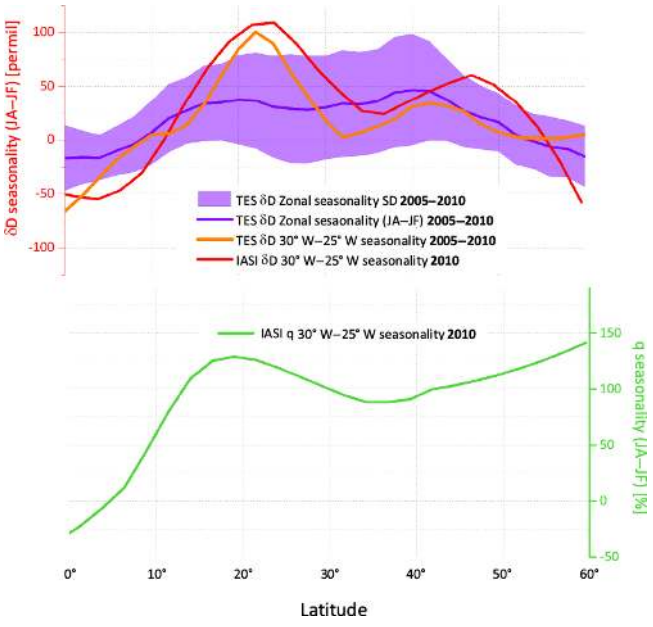

Figure 7. Top panel: global δD zonal seasonality (JA–JF) from 0 to 60° N (purple line) with its associated standard deviation (shaded area) and seasonality found offshore of West Africa (30–25° W, 0–60° N) (orange line) observed by TES for the 2005–2010 period and as observed by IASI seasonality for 2010 (red line). Bottom panel: IASI specific humidity seasonality.

to be thicker and higher off the coast of Africa, between 1 and 5 km above mean sea level, while it is observed between 1 and 3 km during the winter (see Fig. 4 of Tsamalis et al., 2013), i.e. below the altitude of maximum sensitivity of IASI-derived δD products.

4 Inter-annual variations above the CAR

Figure 2 shows that there are significant inter-annual variations observed in the δD signal in the CAR. In this section, we investigate the reasons that could explain this variability.

4.1 Control of the zonal transport

As explained previously, the δD variations are sensitive to the source of water vapour. During summertime, the air masses that reach the CAR have contrasting isotopic signatures and water vapour content: the air masses from the Atlantic are dry and depleted, while the air masses from the African continent are wet and enriched. Schneider et al. (2015) already documented the link between high δD values and the continental origin of the air mass using coinciding observations of dust concentrations. Thus, the origin of the air masses must control δD. Schneider et al. (2015) also demonstrated the influence of Saharan air masses on δD using coinciding observations of dust concentrations and δD–q pairs. In Fig. 9a, we show the correlation between summer (June to August) δD (and q) daily variations and their longitudinal origin for each time step of the backward trajectory analysis. The correlation plot of the δD (and q) daily variations and the longitudinal origin shows that there is a maximum of correlation ($r = 0.68$ with $p < 0.001$) between δD and the longitudinal origin of the air mass going back to 140 h (6 days) prior to the arrival of the air mass at the CAR. Interestingly, this does not correspond to the same maximum for specific humidity variations, which is 60 h prior to the arrival. The daily variations in δD are thus largely controlled by the longitudinal origin of the air mass. The fact that the correlation between δD and the longitudinal origin is the highest going back to 6 days before their arrival compared to 3 days for specific humidity probably translates the memory effect of δD. Indeed, while the specific humidity is reset at its saturation value when there is saturation, δD keeps a record of its previous value before the saturation (Risi et al., 2010).

In Fig. 9b, we present the monthly variations in δD in summer as a function of the ratio of western air masses (air masses that have a longitudinal origin west of 20° W) to the total number of air masses arriving at the CAR. A ratio of 1 indicates that the air masses exclusively come from the Atlantic while a ratio $\ll 1$ indicates that the air masses mainly come from the continent. We found a linear relation ($r = -0.91$, $p < 0.001$) between δD and the ratio indicating that the summer monthly averages of δD observed at the CAR reflect the balance between the two main origins of the air masses. Logically, this translates into the inter-annual seasonal variations in δD shown in Fig. 9c. The inter-annual variability in summer δD values can thus be explained by the relative contributions of air masses coming from the Atlantic and the ones coming from the SHL.

4.2 Control of the mixing fraction

In this section, we assume that the monthly average isotopic composition above the CAR in summer is the result of mixing between upper tropospheric air and boundary layer air, the control of the ratio of the number of the western air masses to the eastern air masses can thus be understood in terms of the mixing fraction of the humid source (f in Eqs. 2 and 3) in a mixing model. This is shown in Fig. 10 in which daily δD–q pairs from June to August are smoothed on a 30-day moving average filter and placed in δD–q diagrams for each year from 2009 to 2013. The observations show a progressive moistening and enrichment along a mixing model from June to August. The mixing model used here involves a dry and depleted term with $\delta\mathrm{D} = -400\,‰$ and $q = 1\,\mathrm{mmol\,mol^{-1}}$ typical of upper tropospheric air masses that mixes with a moist and enriched term, i.e. water vapour evaporated from the ocean with $\delta\mathrm{D} = -70\,‰$ and $q = 14\,\mathrm{mmol\,mol^{-1}}$ (the latter being typical for specific humidities above the Mediterranean). Note that a mixing model involving a wetter, humid term (with the same isotopic composition) could also fit the observations.

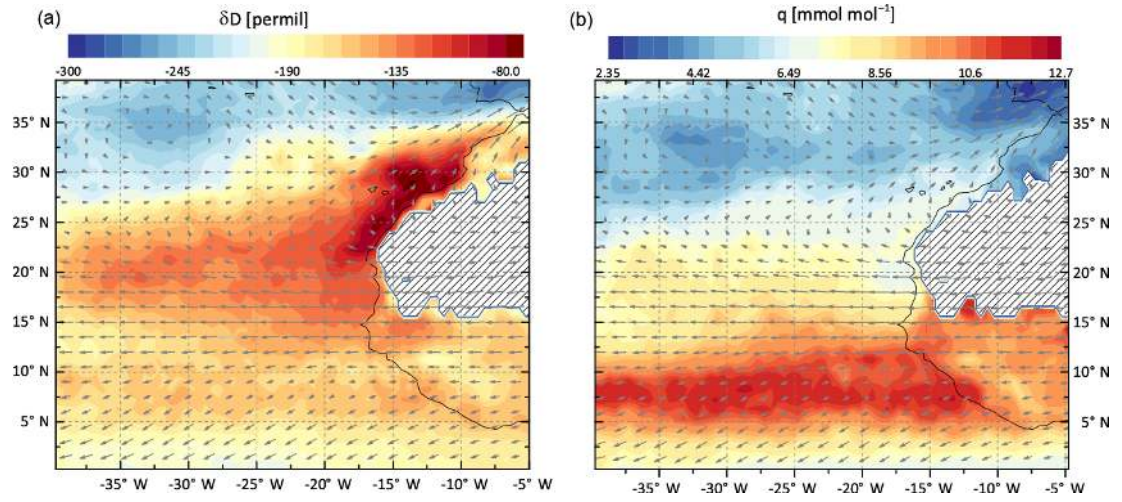

Figure 8. δD **(a)** and q **(b)** distributions from IASI at 4.5 km for July 2012 together with the averaged wind fields at 600 hPa.

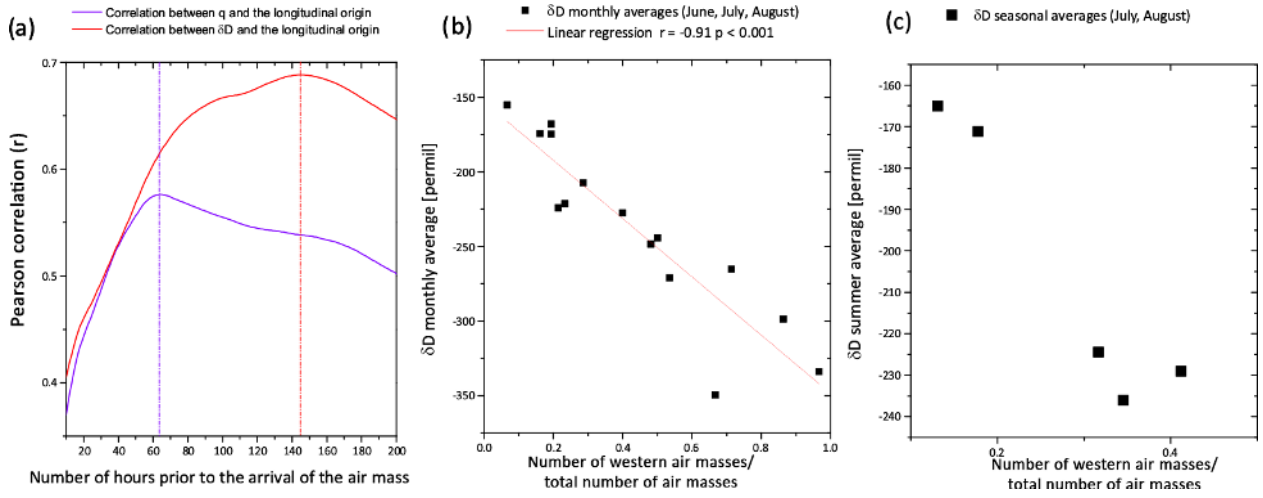

Figure 9. (a) Correlation between δD (red curve) and q (purple curve) daily variations and the longitudinal origin of the air mass at various time steps (number of hours prior to the arrival of the air mass in the CAR). **(b)** δD monthly averages (June, July, and August) as a function of the ratio of the number of air masses arriving from the Atlantic (longitude $< -20°$ W) to the total number of air masses. **(c)** Same as **(b)** but for summer averages (July, August).

This is because δD evaporated from the ocean has very similar values and only the specific humidity varies depending on the latitudinal position of the sea. Hence, the humid term of the mixing model (in orange in Fig. 11) could be associated with tropical boundary layer water vapour or boundary layer water vapour from the Mediterranean region (drier) both being potential sources of water vapour fed into the SHL (so-called SHL ventilation from south or north, respectively; Lavaysse et al., 2009). This means that moisture transported at low level from the oceans and the seas surrounding the continent towards the SHL contribute to the moistening of the free troposphere over the north-eastern Atlantic. The SHL is a key player in this process as the relatively moist and enriched air masses are mixed vertically over the depth of the Saharan ABL before being transported over the ocean due to the divergent, anticyclonic circulation at the top of the SHL. In Fig. 10, the colours indicating the ratio of the number of western air masses to the total number of air masses show that from June to August, as δD increases along the mixing model, the ratio progressively decreases. Assuming constant dry and humid terms, this displacement along the mixing model can be explained by an increase in the mixing fraction (f) in Eqs. (2) and (3). The ratio of the number of western air masses to the total number of air masses thus acts like the mixing fraction in controlling the δD composition of water vapour. The magnitude of the enrichment is important because in the dry member of the mixing model, a small increase in the fraction of boundary layer air acts

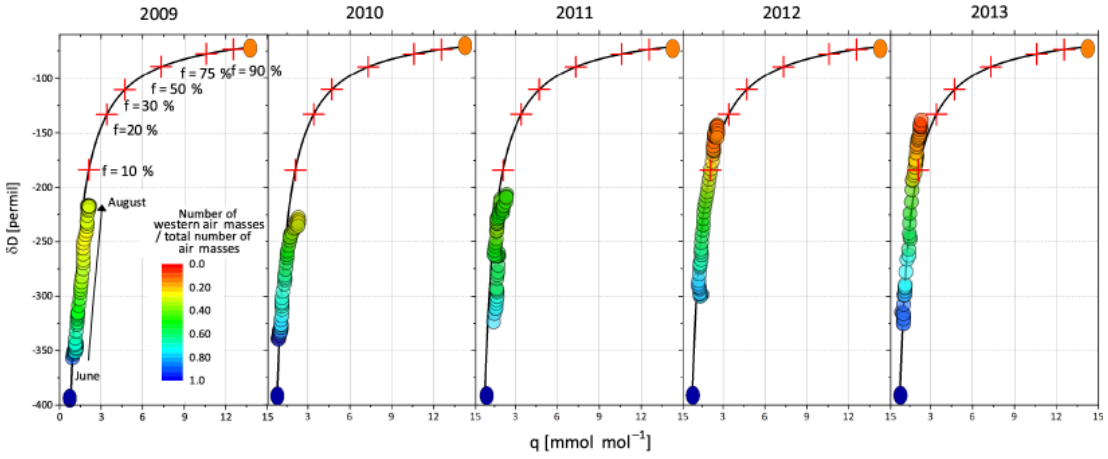

Figure 10. Summer enrichments (from June to August) observed at the CAR from 2009 to 2013 along a mixing model defined by the mixing between upper tropospheric water vapour (UT) and boundary layer vapour above the Mediterranean (MBL). IASI daily observations at 5.5 km are smoothed on a 30-day moving average filter and the corresponding ratios of western air masses to total number of air masses are shown in colour. The 10, 50, 75, and 90 % fractions (f) of MBL of Eqs. (2) and (3) are indicated with the red crosses.

to significantly enrich the resulting mixed air mass (mixing fractions are indicated by the red crosses in Fig. 10). Conversely, the specific humidity increase is small. The summer enrichment observed at the CAR can therefore be interpreted as the progressive increase in the boundary layer air fraction in the mixing as the SHL acts to efficiently blend boundary layer air over increasing depths from June to August, bringing moisture to altitudes at which only upper tropospheric air is observed during the rest of the year. Figure 10 also nicely shows the inter-annual variations observed from 2009 to 2013 as the main origin of the air masses varies. Assuming constant end members of the mixing, the observations suggest that f reaches up to 20 % in 2013 while it is below 10 % from 2009 to 2011.

5 Dehydration pathways in the North Atlantic

Finally, we have analysed the information contained in the isotopic composition of water vapour over the North Atlantic for July 2012. In Fig. 11, we present the δD and q distributions previously shown in Fig. 8 in the δD–q space. The IASI δD–q pairs occupy very distinct domains in the diagram, indicating a wide variety of sources and processes controlling the water vapour above the Atlantic. In this section we aim at disentangling these various sources and processes. To do this, we geographically map the different sources and pathways identified and use simple models describing the isotopic depletion of water vapour (Noone, 2012).

5.1 Sources

The δD–q pairs draw distinctive pathways (Fig. 11) corresponding to the progressive dehydration–moistening and depletion–enrichment from different sources. The latter are

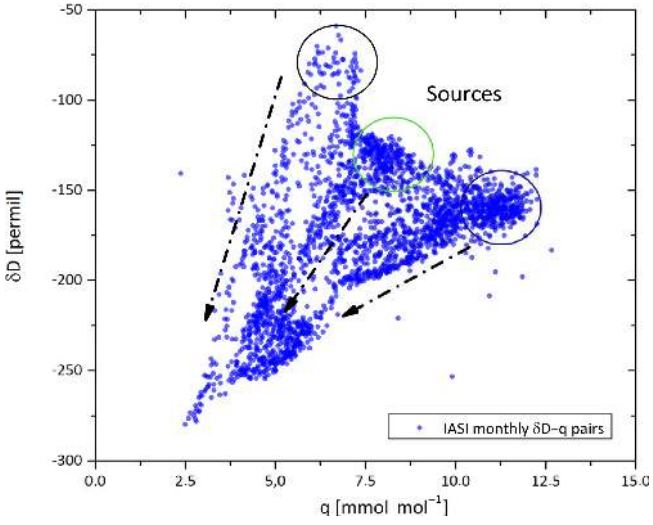

Figure 11. δD–q monthly averages obtained from IASI for July 2012 (see also Fig. 8). Each point represents one location over the North Atlantic. Three sources (circles) and different dehydration pathways (black arrows) are identified. See text for details.

identified as the moist members of the different branches visually identified in the δD–q pair scatter plot. Three different sources of water vapour have been identified according to their positions in the δD–q diagrams. These sources are shown in Fig. 12a and mapped on the spatial distribution of δD in Fig. 12b.

– S1: This source (black squares) is the most enriched and the driest one. It corresponds to water vapour found in a localized area close to the African coast around 26° N and 15° W. We suggest that this enriched source is the direct result of the SHL activity over the Sahara. The dry

convective mixing of water vapour from the Mediterranean Sea with very dry and depleted air from the upper troposphere – as shown with the mixing model in orange – could indeed produce such high enrichment. Note that the humid term could also be more humid but that this would not significantly affect the mixing model.

– S2: This source (blue diamonds) is the most depleted and the wettest one. It corresponds to water vapour found along the ITCZ between 5 and 10° N. This strongly suggests that this source is the result of the convective uplift of water vapour (with condensation) from lower altitudes. In that case, a Rayleigh model describing the depletion of water vapour evaporated from the tropical ocean can explain the δD–q values observed (Fig. 12a, purple line).

– S3: This source with intermediate δD and humidity contents corresponds to a thin longitudinal band along 20° N. This corresponds to the westward transport of dust and aerosol from Africa along the northern border of the AEJ, where the AEJ is strengthened by the SHL anticyclonic circulation (see Fig. 3). In comparison to S1, if we assume that this source is also produced by mixing and that the humid term is similar in both cases, this would mean that the dry term must be different than the mixing, potentially explaining S1. As seen in Fig. 12b, the mixing between Mediterranean boundary layer (MBL) air that has been distilled from tropical water vapour could explain the position of S3 in the δD–q diagram. We thus hypothesize that S3 is the result of mixing between ascending air from the Sahel (MBL) and air from the AEJ, which could be the result of a simple Rayleigh distillation of tropical boundary layer (TBL). Note that, as the S3 exhibits constant δD and humidity values along the northern border of the AEJ, it means that there is no dehydration and no depletion along this longitudinal band, and thus it suggests that there is no or weak mixing along the westward transport above the Atlantic.

In summary, the air masses that circulated within the divergent flow at the top of the SHL show here two different isotopic signatures depending on whether they contribute to strengthening the AEJ over the continent or if they are transported anticyclonically over the Atlantic around the SHL. These two signatures are distinct from the signature of convection found along the ITCZ.

5.2 Pathways

Now that the sources have been identified, we analyse the different moistening and dehydrating pathways visible in the δD–q space from the different sources (Fig. 12c). To dissociate the different pathways we use their position in δD–q space and we also use their geographical position to facilitate the dissociation in both spaces. Note that the sources show quasi constant δD and q values, while the dehydration pathways show an important variability. The dehydration and depletion are mainly latitudinal.

– P1: This pathway describes the dehydration and the rapid depletion of S1. Figure 12d shows that this pathway corresponds to the area in the north of Africa, dominated by wind (see in Figs. 8 and 3) towards Europe where the air is particularly dry and depleted. A mixing model between S1 and a dry term can be used to describe this pathway.

– P2: This pathway corresponds to a small area in between the Canary Islands (S1) and S3. In the δD–q space, these points also lie between S1 and S3. The mixing between S1 and S3 cannot explain the observations as a mixing model between these two terms would produce a hyperbolic line without reproducing the slope observed. Instead, these observations could be explained by the mixing of a constant source such as the MBL, with air becoming more enriched and more humid. This could be explained by a stronger influence of the AEJ and a weaker influence of the subsidence as we get closer to S3. Figure 12e shows how this mechanism could explain the δD–q pairs observed.

– P3: This pathway corresponds to the western part of the North Atlantic where S3 is probably mixed with air from the large-scale subsidence as the end member of the mixing model corresponds to the location of the Azores high.

– P4: This pathway describes the depletion of S2 northward and southward of the ITCZ and can be described by a simple Rayleigh distillation model, which has the characteristics of the tropical boundary layer moisture.

– P5: This pathway is found between S3 and S2 or corresponds to distilled air parcels from S2. The position of the observations in the δD–q space could be explained again by mixing. However, in that case, the enriched source is drier than the humid source and the corresponding mixing model presents an inverse curvature. The blue curves showing the mixing models computed from S3 and S2 or more distilled terms explain the scatter that is observed.

The analysis proposed here suggests that the combined observation of water vapour and its isotopic composition can be very useful in identifying the different sources of humidity, which are key actors of the hydrological and dynamical cycle of the region, and their interactions. It is however impossible to unambiguously assess the processes responsible for the position of δD–q pairs as a combination of different processes can lead to a same δD–q position. Nevertheless,

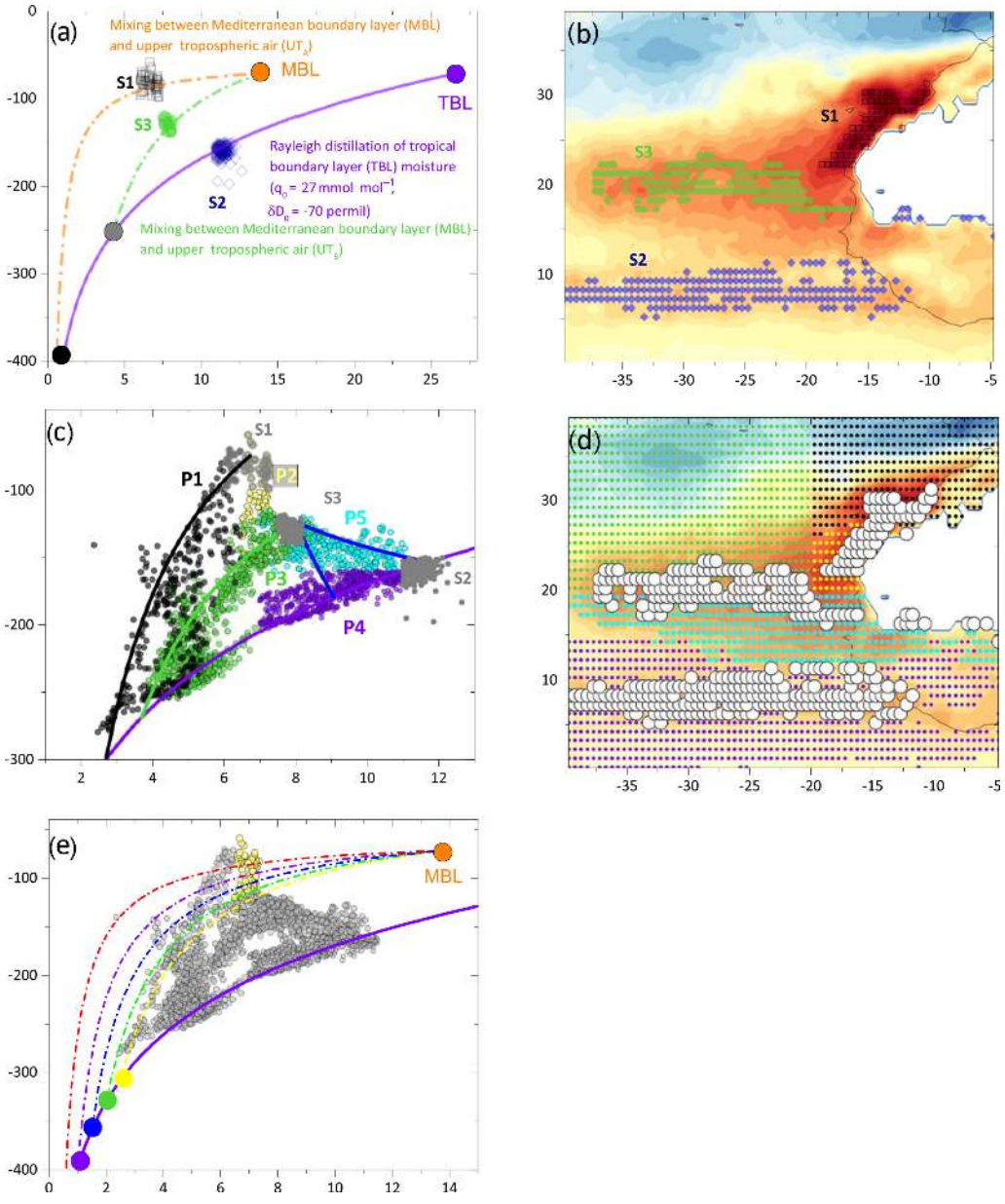

Figure 12. **(a)** δD–q composition of the three main sources identified in the δD–q diagram with a mixing model (orange curve) between upper tropospheric air (black circle) and Mediterranean boundary layer vapour (orange circle); a Rayleigh model from a tropical boundary layer vapour (purple circle); and a mixing model between MBL and water vapour distilled according to the Rayleigh model defined. **(b)** Geographical location of the different sources identified in **(a)**. **(c)** All δD–q pairs for July 2012 together with different mixing models that could explain the variations observed (see text for details); the colours indicate the different pathways identified. The sources identified in **(a)** are shown in grey. **(d)** Geographical location of the different pathways identified in **(c)**. **(e)** Illustration of the mechanism explaining the variations observed in yellow (P2): mixing models between a constant humid term (MBL) and a dry term more and more enriched.

the cohesiveness of our interpretation with the actual understanding of the SHL dynamic suggests that the interpretation is reasonable.

6 Conclusions

In this study we explored δD–q distributions derived from the IASI sounder above the North Atlantic for different time and space scales with the objective of providing an interpretation of the controls of δD in that region. We have shown that the seasonal enrichment of δD observed in the CAR

was closely linked to the influence of the SHL above the Sahara from June to August. By the end of June, the intense surface heating during the summertime period generates deep boundary layers, which can then be transported above the Atlantic within the so-called SAL. When the SAL top reaches the altitude of IASI sensitivity, HDO enrichment is observed over the CAR. We have shown that the influence of the SHL expands far off the coast, suggesting a large influence of the SHL on the isotopic budget and thus on the humidity budget. The summertime δD–q distributions at the CAR are mainly the result of mixing processes between dry and depleted upper tropospheric air with humid and enriched boundary layer air from the oceans and seas surrounding the West African continent. In the summer, the SHL acts to efficiently mix these contrasting sources and transport anomalously moist and enriched air masses (when compared to the rest of the year) over the north-eastern Atlantic Ocean. Interannual variations in δD were also interpreted as the differences in the fraction of western to eastern air masses arriving at the CAR. The combination of δD and q observations from IASI in July 2012, together with the knowledge of the key components of the West African Monsoon system, allowed the interpretation of the variety of processes driving the water budget over the north-eastern Atlantic. More generally this analysis demonstrates the usefulness of δD measurements from IASI as we show it is possible to disentangle the respective contribution of the different sources of water vapour together with their respective interactions.

The demonstrated capabilities of IASI to provide unique observational constraints on the different sources and processes controlling the free tropospheric humidity in the North Atlantic would be useful to evaluate the representation of these sources and processes in isotope-enabled climate models. In particular, the strong isotopic signature associated with the SHL and its interactions with the monsoon and the AEJ could be used to assess the correctness of its representation in climate models.

Data availability. The IASI δD retrieved profiles are available upon request from the lead author (Jean-Lionel.Lacour@latmos.ipsl.fr). TES data are publicly available (https://tes.jpl.nasa.gov/data/). The MERRA data sets were obtained from GES DISC (https://disc.gsfc.nasa.gov/). The ECMWF reanalyses were obtained from http://apps.ecmwf.int/datasets/.

Appendix A: Supplemental backward trajectory analyses

In this appendix we show additional trajectory analyses we conducted to verify that there are no spatial and temporal mismatches in the trajectories due to the large sensitivity layer of IASI and due to the differences in time sampling.

A1 Coherence of air mass trajectories between 3 and 6 km

IASI δD retrievals are sensitive to δD variations over a large vertical layer. The information mostly comes from the free troposphere between 3 and 6 km. In Fig. A1 we show air masses arriving at different altitudes (3.5, 4.5, and 5.5 km) within this layer for the year 2011. Air masses arriving at the different altitudes show similar patterns, indicating that what we show at 5.5 km is also valid for the 3–6 km layer.

A2 Temporal mismatches

Here, we show additional backward trajectory analysis corresponding to different initialization times (9, 12, and 21 UTC). The air parcels show a very coherent trajectory between 9 and 21 UTC.

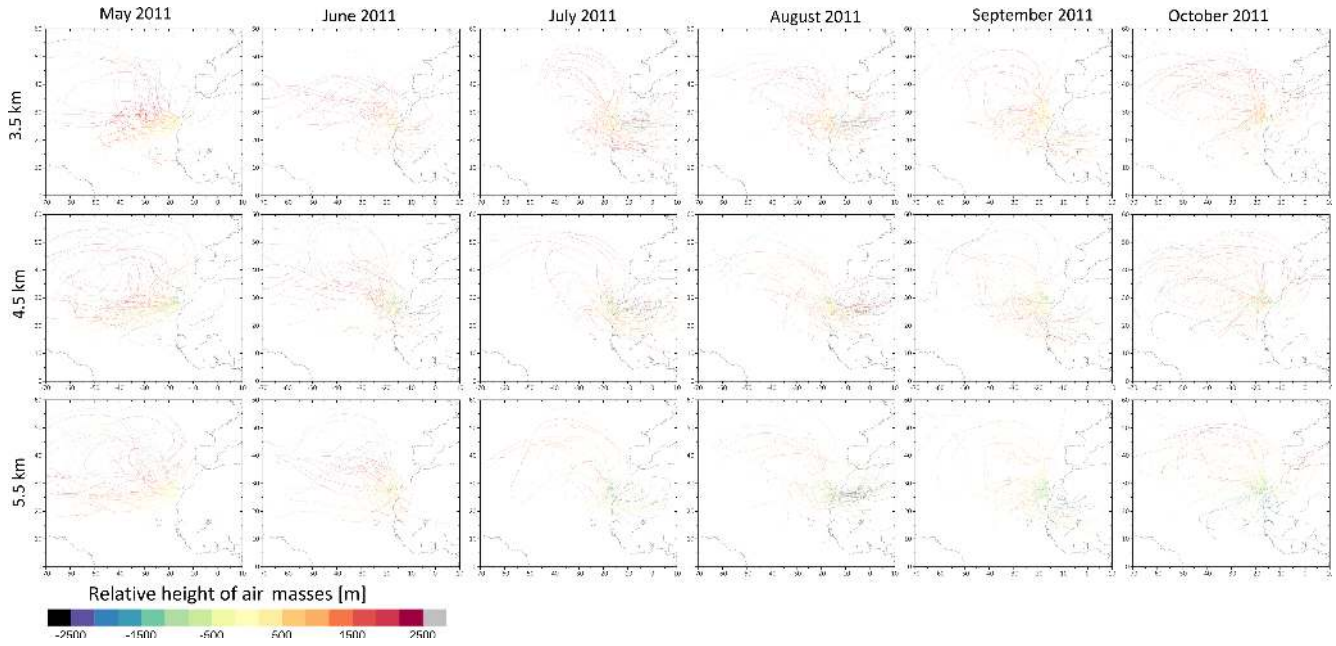

Figure A1. Air masses arriving above the CAR at three different altitudes (3.5, 4.5, and 5.5 km). The trajectories are initialized from three points (26, 28, and 30° N and at the longitudinal centre of the box at 12.00).

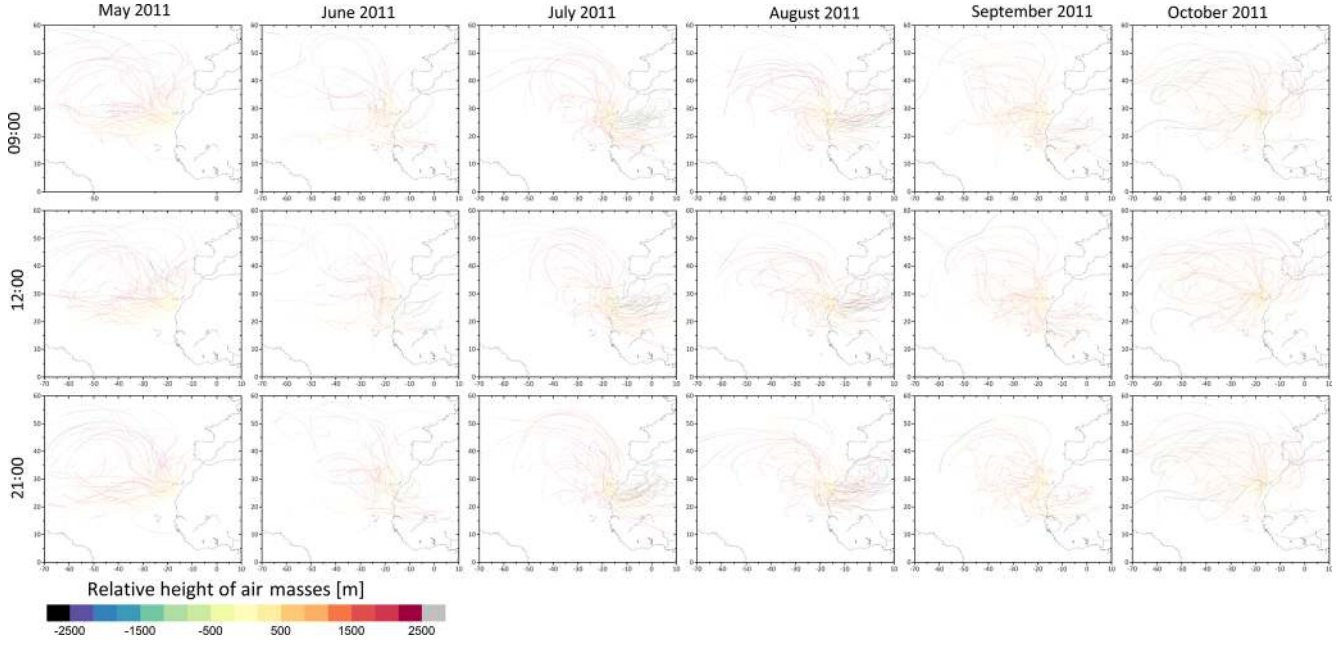

Figure A2. Air masses arriving above the CAR (4.5 km) at three different times (9, 12, and 21 UTC). The trajectories are initialized from three points (26, 28, and 30° N and at the longitudinal centre of the box).

Author contributions. J-LL performed the retrievals of δD from IASI spectra, performed the data analysis, and prepared the paper. CF provided expertise on the SHL and prepared the paper with J-LL. CR provided her expertise on the analysis and corrected the paper. P-FC supervised the first part of this study, in relation to the δD retrievals from IASI. He corrected the paper. CC supervised the second part of this study and corrected the paper.

Competing interests. The authors declare that they have no conflict of interest.

Acknowledgements. IASI has been developed and built under the responsibility of the "Centre National d'Etudes Spatiales" (CNES, France). It is flown on-board the MetOp satellites as part of the EUMETSAT Polar System. The IASI L1 data are received through the EUMETCast near-real-time data distribution service. Jean-Lionel Lacour is grateful to the CNES for the postdoctoral grant. The research in Belgium was funded by the F.R.S.-FNRS, the Belgian State Federal Office for Scientific, Technical and Cultural Affairs (PRODEX arrangement 4000111403 IASI.FLOW). Monthly distribution of δD above the North Atlantic was retrieved thanks to the support provided by the AC-AHC2 project (ANR-15-CE01-0015). Clerbaux is grateful to CNES for scientific collaboration and financial support. The authors thank the two anonymous referees and Matthias Schneider for their helpful comments to improve the paper.

Edited by: Heini Wernli
Reviewed by: two anonymous referees

References

Ben-Ami, Y., Koren, I., and Altaratz, O.: Patterns of North African dust transport over the Atlantic: winter vs. summer, based on CALIPSO first year data, Atmos. Chem. Phys., 9, 7867–7875, https://doi.org/10.5194/acp-9-7867-2009, 2009.

Bonne, J.-L., Steen-Larsen, H. C., Risi, C., Werner, M., Sodemann, H., Lacour, J.-L., Fettweis, X., Cesana, G., Delmotte, M., Cattani, O., Vallelonga, P., Kjæ r, H. A. R., H. A., Clerbaux, C., Sveinbjörnsdóttir, A. E., and Masson-Delmotte, V.: The summer 2012 Greenland heat wave: In situ and remote sensing observations of water vapor isotopic composition during an atmospheric river event, J. Geophys. Res.-Atmos., 120, 2970–2989, https://doi.org/10.1002/2014JD022602, 2015.

Chaboureau, J.-P., Flamant, C., Dauhut, T., Kocha, C., Lafore, J.-P., Lavaysse, C., Marnas, F., Mokhtari, M., Pelon, J., Reinares Martínez, I., Schepanski, K., and Tulet, P.: Fennec dust forecast intercomparison over the Sahara in June 2011, Atmos. Chem. Phys., 16, 6977–6995, https://doi.org/10.5194/acp-16-6977-2016, 2016.

Clerbaux, C., Boynard, A., Clarisse, L., George, M., Hadji-Lazaro, J., Herbin, H., Hurtmans, D., Pommier, M., Razavi, A., Turquety, S., Wespes, C., and Coheur, P.-F.: Monitoring of atmospheric composition using the thermal infrared IASI/MetOp sounder, Atmos. Chem. Phys., 9, 6041–6054, https://doi.org/10.5194/acp-9-6041-2009, 2009.

Dee, D. P., Uppala, S. M., Simmons, A. J., Berrisford, P., Poli, P., Kobayashi, S., Andrae, U., Balmaseda, M. A., Balsamo, G., Bauer, P., Bechtold, P., Beljaars, A. C. M., van de Berg, L., Bidlot, J., Bormann, N., Delsol, C., Dragani, R., Fuentes, M., Geer, A. J., Haimberger, L., Healy, S. B., Hersbach, H., Hólm, E. V., Isaksen, L., Kållberg, P., Köhler, M., Matricardi, M., McNally, A. P., Monge-Sanz, B. M., Morcrette, J.-J., Park, B.-K., Peubey, C., de Rosnay, P., Tavolato, C., Thépaut, J.-N., and Vitart, F.: The ERA-Interim reanalysis: configuration and performance of the data assimilation system, Q. J. Roy. Meteor. Soc., 137, 553–597, https://doi.org/10.1002/qj.828, 2011.

Evan, A. T., Flamant, C., Lavaysse, C., Kocha, C., and Saci, A.: Water Vapor Forced Greenhouse Warming over the Sahara Desert and the Recent Recovery from the Sahelian Drought, J. Climate, 28, 108–123, https://doi.org/10.1175/JCLI-D-14-00039.1, 2015.

Flamant, C., Chaboureau, J.-P., Parker, D. J., Taylor, C. M., Cammas, J.-P., Bock, O., Timouk, F., and Pelon, J.: Airborne observations of the impact of a convective system on the planetary boundary layer thermodynamics and aerosol distribution in the inter-tropical discontinuity region of the West African Monsoon, Q. J. Roy. Meteor. Soc., 133, 1175–1189, https://doi.org/10.1002/qj.97, 2007.

Flamant, C., Lavaysse, C., Todd, M. C., Chaboureau, J.-P., and Pelon, J.: Multi-platform observations of a springtime case of Bodélé and Sudan dust emission, transport and scavenging over West Africa, Q. J. Roy. Meteor. Soc., 135, 413–430, https://doi.org/10.1002/qj.376, 2009.

Frankenberg, C., Yoshimura, K., Warneke, T., Aben, I., Butz, A., Deutscher, N., Griffith, D., Hase, F., Notholt, J., Schneider, M., Schrijver, H., and Rockmann, T.: Dynamic Processes Governing Lower-Tropospheric HDO/H_2O Ratios as Observed from Space and Ground, Science, 325, 1374–1377, https://doi.org/10.1126/science.1173791, 2009.

Galewsky, J. and Hurley, J. V.: An advection-condensation model for subtropical water vapor isotopic ratios, J. Geophys. Res., 115, D16116, https://doi.org/10.1029/2009JD013651, 2010.

Galewsky, J. and Samuels-Crow, K.: Summertime Moisture Transport to the Southern South American Altiplano: Constraints from In Situ Measurements of Water Vapor Isotopic Composition, J. Climate, 28, 2635–2649, https://doi.org/10.1175/JCLI-D-14-00511.1, 2015.

Galewsky, J., Strong, M., and Sharp, Z. D.: Measurements of water vapor D/H ratios from Mauna Kea, Hawaii, and implications for subtropical humidity dynamics, Geophys. Res. Lett., 34, L22808, https://doi.org/10.1029/2007GL031330, 2007.

Galewsky, J., Steen-Larsen, H. C., Field, R. D., Worden, J., Risi, C., and Schneider, M.: Stable isotopes in atmospheric water vapor and applications to the hydrologic cycle, Rev. Geophys., 54, 809–865, https://doi.org/10.1002/2015RG000512, 2016.

González, Y., Schneider, M., Dyroff, C., Rodríguez, S., Christner, E., García, O. E., Cuevas, E., Bustos, J. J., Ramos, R., Guirado-Fuentes, C., Barthlott, S., Wiegele, A., and Sepúlveda, E.: Detecting moisture transport pathways to the subtropical North Atlantic free troposphere using paired H_2O-δD in situ measurements, Atmos. Chem. Phys., 16, 4251–4269, https://doi.org/10.5194/acp-16-4251-2016, 2016.

Held, I. M. and Soden, B. J.: Water vapor feedback and global warming, Annu. Rev. Energy Environ., 25, 441–475, 2000.

Herman, R. L., Cherry, J. E., Young, J., Welker, J. M., Noone, D., Kulawik, S. S., and Worden, J.: Aircraft validation of Aura Tropospheric Emission Spectrometer retrievals of HDO / H_2O, Atmos. Meas. Tech., 7, 3127–3138, https://doi.org/10.5194/amt-7-3127-2014, 2014.

Kleist, D. T., Parrish, D. F., Derber, J. C., Treadon, R., Wu, W.-S., and Lord, S.: Introduction of the GSI into the NCEP Global Data Assimilation System, Weather Forecast., 24, 1691–1705, https://doi.org/10.1175/2009WAF2222201.1, 2009.

Lacour, J.-L., Risi, C., Clarisse, L., Bony, S., Hurtmans, D., Clerbaux, C., and Coheur, P.-F.: Mid-tropospheric δD observations from IASI/MetOp at high spatial and temporal resolution, Atmos. Chem. Phys., 12, 10817–10832, https://doi.org/10.5194/acp-12-10817-2012, 2012.

Lacour, J.-L., Clarisse, L., Worden, J., Schneider, M., Barthlott, S., Hase, F., Risi, C., Clerbaux, C., Hurtmans, D., and Coheur, P.-F.: Cross-validation of IASI/MetOp derived tropospheric δD with TES and ground-based FTIR observations, Atmos. Meas. Tech., 8, 1447–1466, https://doi.org/10.5194/amt-8-1447-2015, 2015.

Lavaysse, C., Flamant, C., Janicot, S., Parker, D., Lafore, J.-P., Sultan, B., and Pelon, J.: Seasonal evolution of the West African heat low: a climatological perspective, Clim. Dynam., 33, 313–330, https://doi.org/10.1007/s00382-009-0553-4, 2009.

Lavaysse, C., Flamant, C., and Janicot, S.: Regional-scale convection patterns during strong and weak phases of the Saharan heat low, Atmos. Sci. Lett., 11, 255–264, https://doi.org/10.1002/asl.284, 2010.

Lavaysse, C., Flamant, C., Evan, A., Janicot, S., and Gaetani, M.: Recent climatological trend of the Saharan heat low and its impact on the West African climate, Clim. Dynam., 47, 3479–3498, https://doi.org/10.1007/s00382-015-2847-z, 2016.

Noone, D.: Pairing measurements of the water vapor isotope ratio with humidity to deduce atmospheric moistening and dehydration in the tropical mid-troposphere, J. Climate, 25, 4476–4494, https://doi.org/10.1175/JCLI-D-11-00582.1, 2012.

Okazaki, A., Satoh, Y., Tremoy, G., Vimeux, F., Scheepmaker, R., and Yoshimura, K.: Interannual variability of isotopic composition in water vapor over western Africa and its relationship to ENSO, Atmos. Chem. Phys., 15, 3193–3204, https://doi.org/10.5194/acp-15-3193-2015, 2015.

Panthou, G., Vischel, T., and Lebel, T.: Recent trends in the regime of extreme rainfall in the Central Sahel, Int. J. Climatol., 34, 3998–4006, https://doi.org/10.1002/joc.3984, 2014.

Pommier, M., Lacour, J.-L., Risi, C., Bréon, F. M., Clerbaux, C., Coheur, P.-F., Gribanov, K., Hurtmans, D., Jouzel, J., and Zakharov, V.: Observation of tropospheric δD by IASI over western Siberia: comparison with a general circulation model, Atmos. Meas. Tech., 7, 1581–1595, https://doi.org/10.5194/amt-7-1581-2014, 2014.

Prospero, J. M. and Carlson, T. N.: Vertical and areal distribution of Saharan dust over the western equatorial north Atlantic Ocean, J. Geophys. Res., 77, 5255–5265, https://doi.org/10.1029/JC077i027p05255, 1972.

Rienecker, M. M., Suarez, M. J., Gelaro, R., Todling, R., Bacmeister, J., Liu, E., Bosilovich, M. G., Schubert, S. D., Takacs, L., Kim, G.-K., Bloom, S., Chen, J., Collins, D., Conaty, A., da Silva, A., Gu, W., Joiner, J., Koster, R. D., Lucchesi, R., Molod, A., Owens, T., Pawson, S., Pegion, P., Redder, C. R., Reichle, R., Robertson, F. R., Ruddick, A. G., Sienkiewicz, M., and Woollen, J.: MERRA: NASA's Modern-Era Retrospective Analysis for Research and Applications, J. Climate, 24, 3624–3648, https://doi.org/10.1175/jcli-d-11-00015.1, 2011.

Risi, C., Bony, S., and Vimeux, F.: Influence of convective processes on the isotopic composition of precipitation and water vapor in the tropics: 2. Physical interpretation of the amount effect, J. Geophys. Res., 113, D19306, https://doi.org/10.1029/2008JD009943, 2008.

Risi, C., Bony, S., Vimeux, F., Frankenberg, C., Noone, D., and Worden, J.: Understanding the Sahelian water budget through the isotopic composition of water vapor and precipitation, J. Geophys. Res., 115, D24110, https://doi.org/10.1029/2010JD014690, 2010.

Risi, C., Noone, D., Worden, J., Frankenberg, C., Stiller, G., Kiefer, M., Funke, B., Walker, K., Bernath, P., Schneider, M., Bony, S., Lee, J., Brown, D., and Sturm, C.: Process-evaluation of tropospheric humidity simulated by general circulation models using water vapor isotopic observations: 2. Using isotopic diagnostics to understand the mid and upper tropospheric moist bias in the tropics and subtropics, J. Geophys. Res., 117, D05304, https://doi.org/10.1029/2011JD016623, 2012.

Risi, C., Noone, D., Frankenberg, C., and Worden, J.: Role of continental recycling in intraseasonal variations of continental moisture as deduced from model simulations and water vapor isotopic measurements, Water Resour. Res., 49, 4136–4156, https://doi.org/10.1002/wrcr.20312, 2013.

Rodgers, C. D.: Inverse methods for atmospheric sounding: theory and practise, World Scientific, 2000.

Rodríguez, S., Alastuey, A., Alonso-Pérez, S., Querol, X., Cuevas, E., Abreu-Afonso, J., Viana, M., Pérez, N., Pandolfi, M., and de la Rosa, J.: Transport of desert dust mixed with North African industrial pollutants in the subtropical Saharan Air Layer, Atmos. Chem. Phys., 11, 6663–6685, https://doi.org/10.5194/acp-11-6663-2011, 2011.

Schneider, M. and Hase, F.: Optimal estimation of tropospheric H_2O and δD with IASI/METOP, Atmos. Chem. Phys., 11, 11207–11220, https://doi.org/10.5194/acp-11-11207-2011, 2011.

Schneider, M., Hase, F., and Blumenstock, T.: Ground-based remote sensing of HDO/H_2O ratio profiles: introduction and validation of an innovative retrieval approach, Atmos. Chem. Phys., 6, 4705–4722, https://doi.org/10.5194/acp-6-4705-2006, 2006.

Schneider, M., González, Y., Dyroff, C., Christner, E., Wiegele, A., Barthlott, S., García, O. E., Sepúlveda, E., Hase, F., Andrey, J., Blumenstock, T., Guirado, C., Ramos, R., and Rodríguez, S.: Empirical validation and proof of added value of MUSICA's tropospheric dD remote sensing products, Atmos. Meas. Tech., 8, 483–503, https://doi.org/10.5194/amt-8-483-2015, 2015.

Schneider, M., Wiegele, A., Barthlott, S., González, Y., Christner, E., Dyroff, C., García, O. E., Hase, F., Blumenstock, T., Sepúlveda, E., Mengistu Tsidu, G., Takele Kenea, S., Rodríguez, S., and Andrey, J.: Accomplishments of the MUSICA project to provide accurate, long-term, global and high-resolution observations of tropospheric {H_2O,δD} pairs – a review, Atmos. Meas. Tech., 9, 2845–2875, https://doi.org/10.5194/amt-9-2845-2016, 2016.

Sherwood, S. C.: Maintenance of the Free-Tropospheric Tropical Water Vapor Distribution. Part I: Clear Regime Bud-

get, J. Climate, 9, 2903–2918, https://doi.org/10.1175/1520-0442(1996)009<2903:MOTFTT>2.0.CO;2, 1996.

Spencer, R. W. and Braswell, W. D.: How Dry is the Tropical Free Troposphere? Implications for Global Warming Theory, B. Am. Meteorol. Soc., 78, 1097–1106, https://doi.org/10.1175/1520-0477(1997)078<1097:HDITTF>2.0.CO;2, 1997.

Stein, A. F., Draxler, R. R., Rolph, G. D., Stunder, B. J. B., Cohen, M. D., and Ngan, F.: NOAA s HYSPLIT Atmospheric Transport and Dispersion Modeling System, B. Am. Meteorol. Soc., 96, 2059–2077, https://doi.org/10.1175/BAMS-D-14-00110.1, 2015.

Sun, D.-Z. and Lindzen, R. S.: Distribution of tropical tropospheric water vapor, J. Atmos. Sci., 50, 1643–1660, 1993.

Thorncroft, C. D. and Blackburn, M.: Maintenance of the African easterly jet, Q. J. Roy. Meteor. Soc., 125, 763–786, https://doi.org/10.1002/qj.49712555502, 1999.

Tsamalis, C., Chédin, A., Pelon, J., and Capelle, V.: The seasonal vertical distribution of the Saharan Air Layer and its modulation by the wind, Atmos. Chem. Phys., 13, 11235–11257, https://doi.org/10.5194/acp-13-11235-2013, 2013.

Tuinenburg, O. A., Risi, C., Lacour, J. L., Schneider, M., Wiegele, A., Worden, J., Kurita, N., Duvel, J. P., Deutscher, N., Bony, S., Coheur, P. F., and Clerbaux, C.: Moist processes during MJO events as diagnosed from water isotopic measurements from the IASI satellite, J. Geophys. Res.-Atmos., 120, 619–636, https://doi.org/10.1002/2015JD023461, 2015.

Wilcox, E. M., Lau, K. M., and Kim, K.-M.: A northward shift of the North Atlantic Ocean Intertropical Convergence Zone in response to summertime Saharan dust outbreaks, Geophys. Res. Lett., 37, l04804, https://doi.org/10.1029/2009GL041774, 2010.

Winker, D. M., Pelon, J., Jr., J. A. C., Ackerman, S. A., Charlson, R. J., Colarco, P. R., Flamant, P., Fu, Q., Hoff, R. M., Kittaka, C., Kubar, T. L., Treut, H. L., McCormick, M. P., Mégie, G., Poole, L., Powell, K., Trepte, C., Vaughan, M. A., and Wielicki, B. A.: The CALIPSO Mission: A Global 3D View of Aerosols and Clouds, B. Am. Meteorol. Soc., 91, 1211–1229, https://doi.org/10.1175/2010BAMS3009.1, 2010.

Worden, J., Bowman, K., Noone, D., Beer, R., Clough, S., Eldering, A., Fisher, B., Goldman, A., Gunson, M., Herman, R., Kulawik, S. S., Lampel, M., Luo, M., Osterman, G., Rinsland, C., Rodgers, C., Sander, S., Shephard, M., and Worden, H.: Tropospheric Emission Spectrometer observations of the tropospheric HDO/H_2O ratio: Estimation approach and characterization, J. Geophys. Res., 111, D16309, https://doi.org/10.1029/2005JD006606, 2006.

Worden, J., Noone, D., and Bowman, K.: Importance of rain evaporation and continental convection in the tropical water cycle, Nature, 445, 528–532, https://doi.org/10.1038/nature05508, 2007.

Worden, J., Kulawik, S., Frankenberg, C., Payne, V., Bowman, K., Cady-Peirara, K., Wecht, K., Lee, J.-E., and Noone, D.: Profiles of CH_4, HDO, H_2O, and N_2O with improved lower tropospheric vertical resolution from Aura TES radiances, Atmos. Meas. Tech., 5, 397–411, https://doi.org/10.5194/amt-5-397-2012, 2012.

Yoshimura, K., Miyoshi, T., and Kanamitsu, M.: Observation system simulation experiments using water vapor isotope information, J. Geophys. Res.-Atmos., 119, 7842–7862, https://doi.org/10.1002/2014JD021662, 2014.